

Synthesis, Characterization and *in vitro* Evaluation of 4-(2-Aminoethyl)benzenesulfonamide Schiff Bases against Arboviruses

Douglas H. Nakahata,^{#,a,b} Carlos E. S. P. Corsino,^{a,c} Guilherme C. de Moraes,^{a,c} Gabriele M. Pereira,^{Ⓜ,b} Álefe B. Cruz,^d Douglas Henrique Pereira,^{d,e} Natasha M. Cassani,^f Uriel Enrique A. Ruiz,^f Igor A. Santos,^f Ana Carolina G. Jardim^{f,g} and Pedro P. Corbi^{Ⓜ,*,b}

^aInstituto de Química, Universidade Federal de Goiás (UFG), 74690-900 Goiânia-GO, Brazil

^bInstituto de Química, Universidade Estadual de Campinas (UNICAMP), 13083-970 Campinas-SP, Brazil

^cInstituto de Física, Universidade Federal de Goiás (UFG), 74690-900 Goiânia-GO, Brazil

^dColegiado de Química, Universidade Federal do Tocantins (UFT), PO Box 66, 77402-970 Gurupi-TO, Brazil

^eDepartamento de Química, Instituto Tecnológico de Aeronáutica (ITA), 12228-900 São José dos Campos-SP, Brazil

^fLaboratório de Pesquisa em Antivirais, Instituto de Ciências Biomédicas, Universidade Federal de Uberlândia (UFU), 38405-302 Uberlândia-MG, Brazil

^gInstituto de Biociências, Humanidades e Ciências Exatas (Ibilce), Universidade Estadual Paulista (UNESP), Campus São José do Rio Preto, 15054-000 São José do Rio Preto-SP, Brazil

This study presents the synthesis and characterization of five Schiff bases derived from the reaction of 4-(2-aminoethyl)-benzenesulfonamide (compound **1**) with corresponding aldehydes, (benzaldehyde, 2-pyridinecarboxaldehyde, 2-quinolinecarboxaldehyde, 8-hydroxy-2-quinolinecarboxaldehyde and 4-imidazolecarboxaldehyde, for compounds **2-6**, respectively). Characterization was performed by various spectroscopic techniques and supported by density functional theory (DFT) calculations. The crystal structures revealed how the substituent groups influenced the present supramolecular interactions. Compounds **1-4** and **6** showed no cytotoxicity to BHK-21 and VERO E6 cells at the highest concentration of 50 $\mu\text{mol L}^{-1}$, while compound **5** was cytotoxic at this concentration. Compound **5** was active against the Chikungunya virus at the concentration of 10 $\mu\text{mol L}^{-1}$, highlighting the effect of the 8-hydroxyquinoline substituent for the antiviral activity. For Zika virus, compound **6** was the only one active at 50 $\mu\text{mol L}^{-1}$. The results suggest the potential of combining sulfonamides with other chemotypes for further development of antiviral agents, especially in the treatment of arboviral diseases.

Keywords: sulfonamides, Schiff bases, antivirals, Zika virus, Chikungunya fever

Introduction

Chikungunya and Zika viral infections have had a global impact, particularly in tropical and subtropical regions, being primarily transmitted by *Aedes* mosquitoes. Patients infected with the Chikungunya virus (CHIKV) usually experience a sudden onset of fever, often accompanied by joint pain. Severe joint pain typically lasts for a few

days but can persist for months or even years, resulting in significant loads on the healthcare system and a profound impact on the quality of life of affected individuals.¹ Meanwhile, Zika virus (ZIKV) infection is characterized by symptoms such as fever, headache, nausea, myalgia, and arthralgia during the acute infection phase. However, one of the most concerning aspects of ZIKV infection is its potential to cause microcephaly in newborns when pregnant women are exposed to the virus.² Regrettably, there are no specific antiviral treatments or approved vaccines available for either CHIKV or ZIKV, which makes controlling outbreaks and managing the long-term health consequences a challenging endeavor in affected regions. Therefore,

*e-mail: ppcorbi@unicamp.br

Editor handled this article: André Galembeck (Guest)

To the memory of Prof Dr Oswaldo Luiz Alves

[#]Current address: Donostia International Physics Center (DIPC), 20018 Donostia, Euskadi, Gipuzkoa, Spain



significant efforts in the field of medicinal chemistry have been directed towards discovering a promising chemotypes for the treatment of CHIKV and ZIKV.³⁻⁶

Sulfonamides are a chemical group containing the [R-SO₂NH-R'] scaffold which have found clinical success as antiviral agents, despite being initially developed as antibacterial agents.⁷ Sulfonamides have found particular effectiveness in the treatment of HIV. As examples, darunavir, fosamprenavir and tipronavir are human immunodeficiency virus (HIV) protease inhibitors approved by the American Food and Drug Administration (FDA). Recently, sulfonamides have been gaining further attention as a promising chemotype for the treatment of other viral infections, including severe acute respiratory coronavirus (SARS-CoV-2), CHIKV and ZIKV.⁸⁻¹¹

Among bioactive sulfonamides, 4-(2-aminoethyl)-benzenesulfonamide (compound **1**, Figure 1) has been explored as a promising scaffold for drug development. It has been reported as a highly selective human carbonic anhydrase (CA) IX inhibitor over the CA II isoform.^{12,13} The human CA IX isoform is overexpressed in several types of solid tumors and they may serve as potential targets of drug development.¹⁴ Schiff bases of compound **1** have been reported in the literature, achieving CA inhibition in the nanomolar range.¹² Radioactive metal complexes containing the motif of compound **1** in the ligand have been designed for positron emission tomography (PET) imaging of tumor hypoxia due to their affinity towards CA IX.¹³

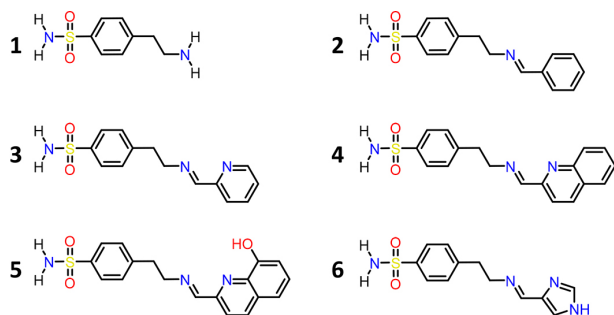


Figure 1. Structural formulas of compounds **1-6** studied in this work.

Schiff bases are formed by condensation of amines and carbonyl compounds. They are versatile molecules with applications spanning coordination chemistry, catalysis, and medicinal chemistry. The Schiff bases can serve as ligands for metal ions, contributing to the creation of unique coordination compounds. In organic synthesis, Schiff bases act as catalysts, enabling various transformations.^{15,16} Recently, molecular docking studies suggested that Schiff bases may be considered as potential inhibitors of SARS-CoV-2 proteins.¹⁷⁻¹⁹ In the same context, there are open opportunities on the development of Schiff bases with

anti-CHIKV and anti-ZIKV activities.²⁰

Herein, we present the synthesis and characterization of a series of compounds obtained by the condensation of 4-(2-aminoethyl)-benzenesulfonamide with several aldehydes, i.e., benzaldehyde (for compound **2**), 2-pyridinecarboxaldehyde (compound **3**), 2-quinolinecarboxaldehyde (compound **4**), 8-hydroxy-2-quinolinecarboxaldehyde (compound **5**) and 4-imidazolecarboxaldehyde (compound **6**) (Figure 1). Compounds **2** and **3** were previously described in the literature, but no antiviral activities were reported so far,^{12,21} while compounds **4-6**, to the best of our knowledge, are new. A systematic study of the crystal structure of the synthesized compounds is presented. Additionally, the electronic structure of the compounds was studied by electronic spectroscopy and supported by density functional theory (DFT) calculations. Finally, the activity of the compounds over CHIKV and ZIKV was investigated.

Experimental

Reagents and equipment

4-(2-Aminoethyl)-benzenesulfonamide (compound **1**, 99%), benzaldehyde ($\geq 99\%$), 2-pyridinecarboxaldehyde (99%), 2-quinolinecarboxaldehyde (97%), 8-hydroxy-2-quinolinecarboxaldehyde ($\geq 98.0\%$) and 4-imidazolecarboxaldehyde (98%) were acquired from Sigma-Aldrich laboratories (USA). All chemicals were of analytical grade and used without further purification.

Elemental analyses were performed on a PerkinElmer 2400 CHNS/O Analyzer. Electronic spectra of ethanolic solutions of the compounds were acquired within the 190-1100 nm range using a 1.0 cm (path length) quartz cuvette in a diode array HP8453 UV/Visible absorption spectrophotometer. Electrospray ionization quadrupole time-of-flight mass spectrometric (ESI-QTOF-MS) measurements were conducted in a Waters Synapt HDMS instrument. The samples were analyzed in a 1:1 methanol:water solution with addition of 0.10% (v/v) formic acid. Each sample was directly infused into the ESI source of the instrument and analyzed in the positive mode, with capillary potential of 3.50 kV, source temperature of 150 °C and nitrogen gas for desolvation. The ¹H and ¹³C nuclear magnetic resonance (NMR) spectra were recorded in Bruker Avance III 400 or 500 MHz spectrometers. The compounds were dissolved in deuterated dimethylsulfoxide (DMSO-*d*₆) and the ¹H and ¹³C signals from solvent residual peak were set to 2.50 and 39.52 ppm, respectively.²² Thermogravimetric analyses were performed on a simultaneous TG/DTA DTG

60/60H (Shimadzu) thermoanalyzer, using the following conditions: temperature range from 25 to 800 °C, heating rate of 10 °C min⁻¹ and synthetic air flow (20 mL min⁻¹).

Data collections for the single crystals of compounds **2-6** were performed with a Bruker Apex II CCD diffractometer with graphite monochromated Mo K α ($\lambda = 0.71073$ Å) or Cu K α ($\lambda = 1.5418$ Å) radiations. Unit cell dimensions and orientation matrices were determined by least squares refinement of the reflections. The data were indexed and scaled with the Apex II Suite.²³ Bruker SAINT²⁴ and SADABS²⁵ were used to integrate and for absorption correction, respectively. The structures were solved with ShelXT using intrinsic phasing and refined with ShelXL²⁶ in Olex2 (v. 1.2.10).²⁷ The nonhydrogen atoms were refined anisotropically. The hydrogen atoms were added to the structure in idealized positions and refined according to the riding model, except for those from -NH₂ (compounds **2-6**), -OH (compound **5**) and -NH (imidazole, compound **6**) groups involved in hydrogen bonding. Molecular graphics were obtained using Mercury (v. 3.10)²⁸ and Olex2. Crystallographic information for compounds **2-6** can be found in Table S1 (Supplementary Information (SI) section).

Syntheses

The Schiff bases were prepared using the same general method, unless stated otherwise. In summary, 2.0 mmol of the corresponding aldehydes (the solid aldehydes of **4** and **5** were dissolved in ethanol) were added to a flask containing 2.0 mmol of 4-(2-aminoethyl)-benzenesulfonamide, dissolved in warm ethanol and the final volumes were 20 mL. The reaction mixtures were refluxed for 4 h under stirring. The solids (see details for each compound below) were isolated by filtration, washed with cold ethanol and dried under vacuum. Purification of the prepared compounds was performed by recrystallization in methanol or ethanol.

Compound 2

A white solid appeared after cooling the reaction system for 12 h, Yield: 73%, calcd. for C₁₅H₁₆N₂O₂S (%): C, 62.5; H, 5.59; N, 9.71; experimental (%): C, 61.4; H, 5.03; N, 9.79; ¹H NMR (400 MHz, DMSO-*d*₆) δ 8.62 (s, 1H), 7.73 (m, 4H), 7.45 (m, 5H), 7.28 (s, 2H), 3.84 (t, 2H, *J* 7.2 Hz), 3.02 (t, 2H, *J* 7.2 Hz); ¹³C NMR (100 MHz, DMSO-*d*₆) δ 161.3, 144.2, 141.9, 136.0, 130.6, 129.3, 128.6, 127.8, 125.6, 61.3, 36.5; HRMS (ESI+) *m/z*, calcd. for C₁₅H₁₇N₂O₂S⁺ [M + H]⁺: 289.1005, found: 289.1002. Single-crystals suitable for diffraction were obtained by recrystallization of the precipitate in methanol.

Compound 3

A yellow crystalline solid appeared after cooling the reaction system for 12 h. Yield: 75%; calcd. for C₁₄H₁₅N₃O₂S (%): C, 58.1; H, 5.23; N, 14.5; experimental (%): C, 57.8; H, 5.17; N, 14.3; ¹H NMR (500 MHz, DMSO-*d*₆) δ 8.62 (ddd, 1H, 0.8, 1.6, 4.8 Hz), 8.29 (s, 1H), 7.94 (1H, dt, *J* 8.0, 1.2 Hz), 7.87 (td, 1H, *J* 8.0, 1.6 Hz), 7.73 (d, 2H, *J* 8.4 Hz), 7.46 (d, 2H, *J* 8.4 Hz), 7.45 (overlapped, 1H), 7.27 (br, 2H), 3.91 (td, 2H, *J* 7.2, 1.2 Hz), 3.04 (t, 2H, *J* 7.2 Hz); ¹³C NMR (125 MHz, DMSO-*d*₆) δ 162.4, 154.0, 149.4, 144.0, 142.0, 136.9, 129.3, 125.6, 125.2, 120.4, 61.1, 36.3; HRMS (ESI+) *m/z*, calcd. for C₁₄H₁₆N₃O₂S⁺ [M + H]⁺: 290.0963, found: 290.0912. Single-crystals suitable for diffraction studies were obtained by slow evaporation of the filtrate of the synthesis.

Compound 4

A yellow powder precipitated after cooling the reaction system for 12 h. Yield: 90%; calcd. for C₁₈H₁₇N₃O₂S (%): C, 63.7; H, 5.05; N, 12.4; experimental (%): C, 63.0; H, 4.90; N, 12.2; ¹H NMR (500 MHz, DMSO-*d*₆) δ 8.47 (s, 1H), 8.43 (d, 1H, *J* 8.4 Hz), 8.05 (m, 3H), 7.82 (m, 1H), 7.76 (d, 2H, *J* 8.0 Hz), 7.67 (ddd, 1H, m), 7.49 (d, 2H, *J* 8.0 Hz), 7.28 (br, 2H), 4.00 (td, 2H, *J* 7.2, 0.8 Hz), 3.10 (t, 2H, *J* 7.2 Hz); ¹³C NMR (125 MHz, DMSO-*d*₆) δ 162.7, 154.3, 147.2, 144.01, 142.0, 136.9, 130.1, 129.4, 129.1, 128.3, 128.0, 127.6, 125.6, 117.8, 61.2, 36.2; HRMS (ESI+) *m/z*, calcd. for C₁₈H₁₈N₃O₂S⁺ [M + H]⁺: 340.1120, found: 340.1019. Single-crystals suitable for diffraction studies were obtained by slow evaporation of the filtrate of the synthesis.

Compound 5

This compound was synthesized by the same method described before, but with the use of 1.0 mmol of each reactant and total volume of 10 mL of ethanol. A yellow solid precipitated during the synthesis. Yield: 65%; calcd. for C₁₈H₁₇N₃O₃S (%): C, 60.8; H, 4.82; N, 11.8; experimental (%): C, 60.3; H, 4.29; N, 11.9; ¹H NMR (400 MHz, DMSO-*d*₆) δ 9.72 (br, 1H), 8.46 (s, 1H), 8.34 (d, 1H, *J* 8.4 Hz), 8.05 (d, 1H, *J* 8.4 Hz), 7.74 (d, 2H, *J* 8.4 Hz), 7.48 (d, 2H, *J* 8.4 Hz), 7.48 (overlapped, 1H), 7.42 (dd, 1H, *J* 7.6, 1.2 Hz), 7.27 (br, 2H), 7.13 (dd, 1H, *J* 7.6, 1.2 Hz), 3.99 (t, 2H, *J* 7.2 Hz), 3.10 (t, 2H, *J* 7.2 Hz); ¹³C NMR (100 MHz, DMSO-*d*₆) δ 162.5, 153.6, 152.2, 144.0, 142.0, 137.9, 136.8, 129.4, 129.3, 128.7, 125.6, 118.0, 117.8, 112.1, 61.4, 36.3; HRMS (ESI+) *m/z*, calcd. for C₁₈H₁₈N₃O₃S⁺ [M + H]⁺: 356.1069, found: 356.1013. Single-crystals suitable for diffraction were obtained by recrystallization of the precipitate in ethanol.

Compound 6

A light-yellow powder precipitated after cooling the reaction system for 12 h. Yield 51%; calcd. for $C_{12}H_{14}N_4O_2S$ (%): C, 51.8; H, 5.01; N, 20.1; experimental (%): C, 51.8; H, 5.28; N, 20.0; 1H NMR (400 MHz, DMSO- d_6) δ 12.42 (s, 1H), 8.14 (s, 1H), 7.73 (d, 2H, J 8.4 Hz), 7.69 (s, 1H), 7.43 (d, 2H, J 8.4 Hz), 7.28 (s, 2H), 3.76 (t, 2H, J 7.2 Hz), 2.97 (t, 2H, J 7.2 Hz); ^{13}C NMR (100 MHz, DMSO- d_6) δ 144.26, 141.88, 129.28, 125.57, 61.44, 36.69; HRMS (ESI+) m/z , calcd. for $C_{12}H_{15}N_4O_2S^+$ [M + H] $^+$: 279.0916, found: 279.1414. Single-crystals suitable for diffraction studies were obtained by slow evaporation of the supernatant of the synthesis after one week of stand.

Molecular modeling

All calculations were performed using the Gaussian 09 program²⁹ and the structures were generated and analyzed by GaussView software.³⁰ Optimization and vibrational frequency calculations were performed using density functional theory with the hybrid functional B3LYP³¹⁻³⁴ and basis set 6-311++G(3df,3pd).³⁵⁻³⁷ No imaginary frequencies were found, showing that the structures were at minimum energy.

The energy values of highest occupied molecular orbital (HOMO) and lowest unoccupied molecular orbital (LUMO) were generated and the energy gap for the chemical species was calculated according to equation 1:

$$\Delta E_{GAP} = E_{LUMO} - E_{HOMO} \quad (1)$$

The energies of the HOMO and LUMO were used to obtain chemical hardness (η), chemical softness (S), chemical potential (μ), electronegativity (χ) and electrophilicity index (ω),^{38,39} equations 2-5:

$$\eta = (E_{HOMO} - E_{LUMO}) \quad (2)$$

$$S = \frac{1}{\eta} \quad (3)$$

$$\mu = \frac{(E_{HOMO} + E_{LUMO})}{2} = -\chi \quad (4)$$

$$\omega = \frac{\mu^2}{2\eta} \quad (5)$$

For the UV-Vis calculations, the structural data of the crystals (compounds **2-6**) were used together with the matrix optimized for compound **1**. The time-dependent density functional theory (TD-DFT) with the

CAM-B3LYP⁴⁰ functional and basis set 6-311++G(3df,3pd) were used and 10 excited states evaluated. The ethanol solvent effect was employed using the solvation model based on density (SMD) implicit solvent model⁴¹ and the scaling factor 0.966⁴² was used in the TD-DFT calculations.

Cell viability by MTT assay

Cell viability was measured by the MTT (3-(4,5-dimethylthiazol-2-yl)-2,5-diphenyl tetrazolium bromide) assay. BHK-21 cells (fibroblasts derived from Syrian golden hamster kidney; ATCC CCL-10) or Vero E6 cells (kidney tissue derived from a normal adult African green monkey, ATCC E6) were cultured in 48-well plate and treated with different concentrations of each compound for 16 h at 37 °C with 5% of CO₂. After treatment, media containing compound was removed from and MTT at 1 mg mL⁻¹ solution was added to each well, incubated for 30 min and replaced with 100 μ L of DMSO to solubilize the formazan crystals. The absorbance was measured at 490 nm on Glomax microplate reader (Promega). Cell viability was calculated according to the equation (T/C) \times 100%, which T and C represented the optical density of the treated well and control groups, respectively. DMSO was used as non-treated control.

Anti-CHIKV activity

The CHIKV expressing *nanoluciferase* reporter (CHIKV-*nanoluc*) used for the antiviral assays is based on the CHIKV isolate LR2006OPY1 (East/Central/South African genotype). The cDNA of CHIKV-*nanoluc* was placed under the control of a cytomegalovirus (CMV) promoter.^{43,44} To determine viral titers, 1 \times 10⁵ BHK-21 cells were seeded in each of 24 wells plate 24 h prior to the infection. Then, the cells were infected with ten-fold serial dilutions of CHIKV-*nanoluc* for 1 h at 37 °C. The inoculums were removed, cells were washed with phosphate buffer saline (PBS) to remove the unbound virus, and added of fresh medium supplemented with 1% penicillin, 1% streptomycin, 2% fetal bovine serum (FBS) and 1% carboxymethyl cellulose (CMC). Infected cells were incubated for 2 days in a humidified 5% CO₂ incubator at 37 °C, followed by fixation with 4% formaldehyde and stained with 0.5% violet crystal. The viral foci were counted to determine viral titer, which was presented in plaque-forming units *per* milliliter (PFU mL⁻¹).

BHK-21 cells were seeded at density of 5 \times 10⁴ cells *per* well into 48-well plates 24 h prior to the infection. CHIKV-*nanoluc* at a multiplicity of infection (MOI) of 0.1 and the compound were simultaneously added to cells. Samples were harvested in *Renilla*-luciferase lysis buffer

(Promega) at 16 h post-infection (h.p.i.) and virus replication was quantified by measuring nanoluciferase activity using the *Renilla*-luciferase Assay System (Promega). Data were analyzed for normal distribution, in order to demonstrated if a parametric or nonparametric test should be applied. Then, the one-way analysis of variance (ANOVA) or Mann-Whitney test was used to compare the treatment with each compound with the DMSO control, using $p < 0.05$.

Anti-ZIKV activity

A wild type ZIKV isolate from a clinical sample of a patient in Brazil (ZIKV_{PE243})⁴⁵ was amplified employing infected Vero E6 cells in 75 cm² flask for 3 days. Then, the viral supernatant was collected and stored at -80 °C. To determine viral titers, 5×10^3 Vero E6 cells were seeded in each of 96 wells plate 24 h prior to the infection. Cells were infected with 10-fold serially dilution of ZIKV_{PE243} and incubated for 72 h in a humidified 5% CO₂ incubator at 37 °C. Then, cells were fixed with 4% formaldehyde, washed with PBS followed by the addition of blocking buffer (BB) containing 0.1% Triton X-100 (Vetec Labs), 0.2% bovine albumin (BSA) and PBS for 30 min, to perform immunofluorescence assay.⁴⁶ Images were analyzed at EVOs Cell Imaging Systems Fluorescence Microscopy (Thermo Fisher Scientific) and focus of infection were counted and measured as focus forming unit *per* milliliter (FFU mL⁻¹).

To assess the antiviral activity of each compound, Vero E6 cells were seeded at a density of 5×10^3 cells *per* well into 96 well plates for 24 h and infected with ZIKV_{PE243} at a MOI of 0.01 FFU cell⁻¹ in the presence of each compound at the established non-cytotoxic concentration. Cells were fixed with 4% formaldehyde, washed with PBS and BB added for immunofluorescence assay and FFU were counted. Data were analyzed for normal distribution to demonstrate the applicability of the parametric or the nonparametric test. Then, two-way ANOVA test was employed to compare the treatment of each compound with the DMSO as control, with a $p < 0.05$.

CHIKV and ZIKV infections for antiviral assays were performed at a BSL-2 laboratory under the authorization number CBQ: 163/02 and process SEI: 01,245.006267/2022-14 from the National Technical Commission for Biosecurity from Brazil (CTNBio).

Results and Discussion

Synthesis and characterization

The compounds **2-6** were synthesized via reaction of compound **1** with the appropriate aldehyde, in ethanol under

reflux. Elemental analysis of all compounds was consistent with the proposed formulae, without any solvent adducts. TG/DTA analysis showed no mass loss below 200 °C for any of the compounds (Figures S1 and S2, SI section), while melting occurred between 153 °C (compound **1**) and 186 °C (compound **5**). The differences in melting temperature could be directly related to hydrogen bonding patterns and other supramolecular interactions present for each compound, as observed in the crystal structures.

¹H NMR spectra of the Schiff bases also revealed formation of the imine due to the presence of a $-CH-$ proton in the 8.0-8.3 ppm range (see Figure 2). Depending on the nature of the substituent aromatic ring, the chemical shift of the $-CH-$ proton and of the $-CH_2-$ protons varied accordingly. The phenyl and pyridyl substituents led to similar chemical shifts (8.29 ppm for the $-CH-$ proton), and the same occurred for the quinolynyl and 8-hydroxyquinolynyl ones (8.46 ppm). The 4-imidazolyl substitution led to the most distinct electronic effects, leading to the most shielded protons (8.14 ppm for the $-CH-$ proton). Full ¹H and ¹³C NMR spectra and signal attribution are provided in the SI section (Figures S3-S12).

Crystal structures

Single-crystals suitable for X-ray diffraction analysis were obtained for all synthesized Schiff bases. The asymmetric units of the compounds **2-6**, shown in Figure 3, are consistent with the proposed condensation reaction of 4-(2-aminoethyl)-benzenesulfonamide with the corresponding aldehydes, which led to the formation of imines. The N(2)–C(9) bond length is a probe for the formation of the imine, since its value should be within the C=N average double bond range of 1.279(8) Å.⁴⁷ For compounds **2-6**, the values were 1.265(2), 1.266(2), 1.264(2), 1.270(2) Å and 1.267(2), respectively. The bond lengths of the five compounds are consistent with those previously reported for similar structures based on the 4-(2-aminoethyl)benzenesulfonamide motif.⁴⁸⁻⁵⁰

The main supramolecular interactions identified for the crystal structures are presented in Table 1. Compound **2** was previously reported in the literature,¹² but its crystal structure was not provided. It was used here as the prototype in the structural analysis of intermolecular interactions of the aromatic derivatives. The main intermolecular interaction seen for **2** were hydrogen bonds, where the $-NH_2$ from the sulfonamide acts as hydrogen bond donor to a nitrogen of an imine, N(2), and one oxygen atom from the sulfonamide group, O(2). Additionally, only one significant C–H... π interaction was observed, with no relevant π ... π interactions (with Cg...Cg distances ≤ 4.0 Å) identified.

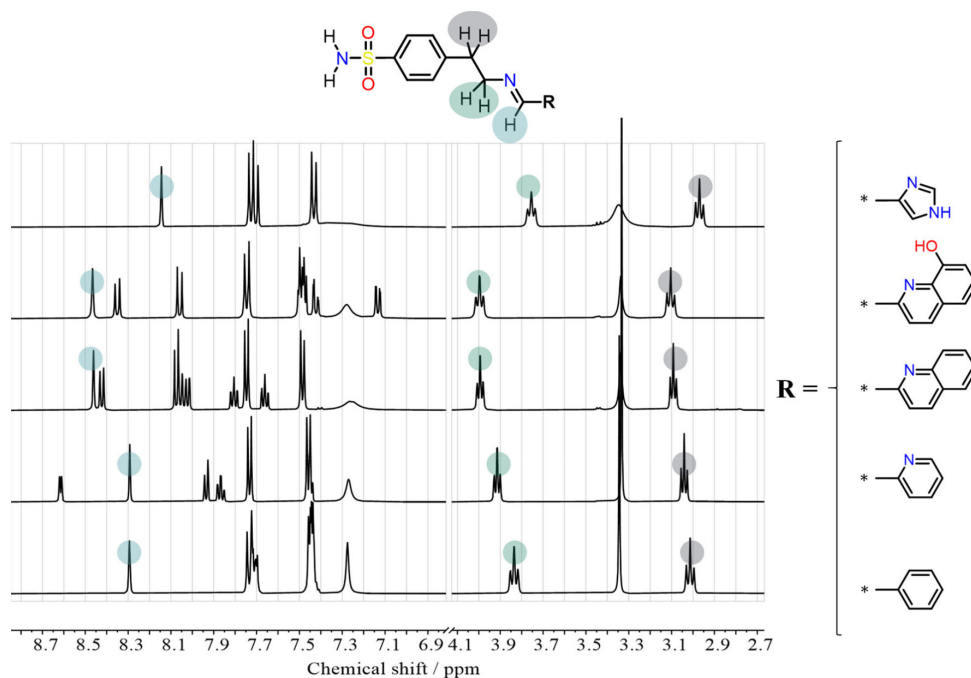


Figure 2. ^1H NMR spectra of compounds **2-6** with the aromatic and aliphatic regions, highlighting diagnostic signals common for all structures. Spectra were acquired in $\text{DMSO-}d_6$ at 400 MHz (for compounds **2**, **5** and **6**) or 500 MHz (for compounds **3** and **4**).

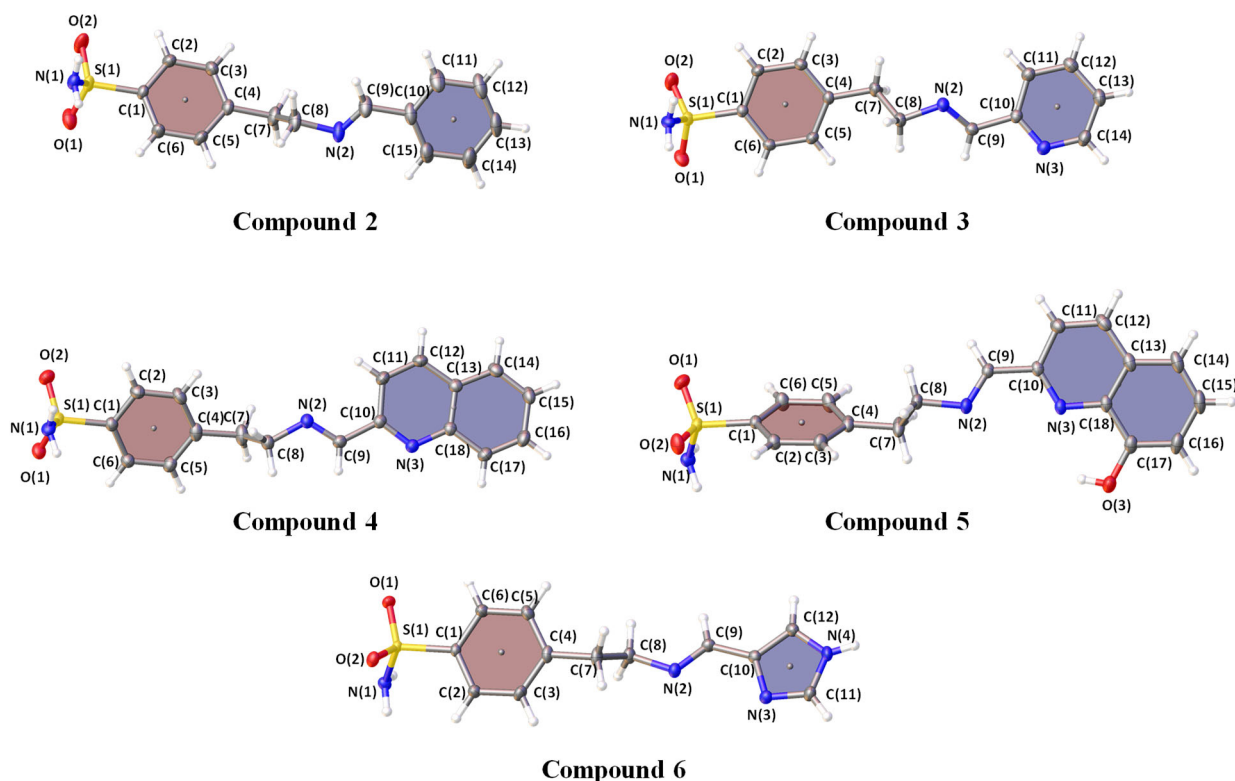


Figure 3. Molecular view of compounds **2-6**. Displacement ellipsoids are drawn at the 50% probability level. The hydrogen atoms were not labeled, for clarity. The red and blue aromatic rings were highlighted with centroids corresponding to Cg1 and Cg2 (Table 1), respectively, for each crystal structure.

Meanwhile, compounds **3** and **4** have a N-heterocyclic substituent in the form the pyridyl and quinolinyl rings that acted as hydrogen bond acceptors. Therefore, in these two crystal structures, only nitrogen atoms acted as hydrogen

bond acceptors to the $-\text{NH}_2$ group, in contrast to what was observed for compound **2**.

Compound **5** presented the most complex array of supramolecular interactions, especially due to its hydrogen

bond donor (–OH group) in the 8-hydroxyquinoline ring. The shortest $\pi\cdots\pi$ interaction was observed for this crystal structure, where two 8-hydroxyquinoline rings stacked in an offset manner (Cg \cdots Cg distance of 3.6870(7) Å). Finally, compound **6** has an imidazole group, which acted as a hydrogen bond acceptor (of the –NH₂ group) and donor (to one oxygen atom of the sulfonamide group).

Molecular modeling

To gain further insights into the electronic properties of the compounds, DFT calculations were performed. To verify the accuracy of the method used and simulate the structure of compound **1**, the structures of compounds **2–6** were

optimized at B3LYP/6-311++G(3df,3pd) level and the results were compared with crystal data (Table S2, SI section). From the results presented in Table S2, it is possible to infer that the calculated structures resulted in geometrical parameters that are consistent with experimental data and, therefore, the level of theory could be used to simulate compound **1**. To further understand the electronic structure of compounds **1–6**, their frontier molecular orbitals and the energy gap have been calculated and the results are represented in Figure 4. The HOMO and LUMO are the most important molecular orbitals because they explain the chemical behavior, bioactivity and physical properties of a molecule.⁵¹ Well-defined π orbitals were observed in all cases, highlighted by the absence of electronic probability density in the sulfonamide group in

Table 1. Geometrical parameters of the supramolecular interactions present in the crystal structures of **2–6**

D–H \cdots A	D–H / Å	H \cdots A / Å	D \cdots A / Å	D–H \cdots A / degree	Symmetry code
Compound 2					
N(1)–H(1A) \cdots N(2)	0.82(3)	2.12(3)	2.918(2)	164(3)	1/2+x, –1/2+y, z
N(1)–H(1B) \cdots O(2)	0.84(3)	2.04(3)	2.843(2)	160(3)	x, 1–y, 1/2+z
C(7)–H(7A) \cdots O(1)	0.99	2.59	3.550(2)	163	–1/2+x, 3/2–y, –1/2+z
π -Interaction	Distance / Å	γ^a / degree			
C(5)–H(5) $\cdots\pi$ (Cg2)	2.72	11.04			1/2+x, 3/2–y, 1/2+z
Compound 3					
N(1)–H(1A) \cdots N(2)	0.865(16)	2.084(17)	2.9426(17)	171.8(17)	1/2–x, –1/2+y, 1/2–z
N(1)–H(1B) \cdots N(3)	0.86(2)	2.07(2)	2.9029(17)	164.5(17)	1–x, 1–y, 1–z
C(3)–H(3) \cdots O(1)	0.95	2.50	3.2242(17)	133	–1/2+x, 1/2–y, –1/2+z
C(12)–H(12) \cdots O(2)	0.95	2.51	3.2290(18)	132	1–x, 1–y, –z
C(13)–H(13) \cdots O(2)	0.95	2.50	3.3076(17)	143	x, 1+y, z
π -Interaction	Distance / Å	β^b / degree			
π (Cg1) $\cdots\pi$ (Cg2)	3.8771(8)	19.2			1/2–x, 1/2+y, 1/2–z
Compound 4					
N(1)–H(1A) \cdots N(3)	0.847(17)	2.116(16)	2.9495(18)	167.8(16)	–1+x, 3/2–y, 1/2+z
N(1)–H(1B) \cdots N(2)	0.87(2)	2.19(2)	3.0179(18)	160.4(18)	x, 3/2–y, 1/2+z
C(8)–H(8A) \cdots O(1)	0.99	2.57	3.3947(18)	141	x, 3/2–y, –1/2+z
C(14)–H(14) \cdots O(1)	0.95	2.51	3.1817(18)	128	x, y, –1+z
C(16)–H(16) \cdots O(1)	0.95	2.51	3.4154(19)	160	1+x, y, –1+z
π -Interaction	Distance / Å	β / degree			
π (Cg1) $\cdots\pi$ (Cg1)	3.9138(9)	20.9			–x, 1–y, 2–z
Compound 5					
N(1)–H(1A) \cdots N(2)	0.87(2)	2.393(19)	3.2141(18)	157.0(15)	1–x, 1–y, 1–z
N(1)–H(1B) \cdots N(2)	0.874(18)	2.289(18)	3.0863(16)	151.8(16)	x, y, –1+z
O(3)–H(3) \cdots N(1)	0.83(2)	2.26(2)	3.0179(15)	151(2)	1–x, 1–y, 1–z
C(8)–H(8A) \cdots O(1)	0.99	2.47	3.3030(18)	142	2–x, 1–y, 1–z
C(9)–H(9) \cdots O(1)	0.95	2.59	3.4413(17)	150	2–x, 1–y, 1–z
C(12)–H(12) \cdots O(2)	0.95	2.47	3.3559(17)	156	x, –1+y, 1+z
π -Interaction	Distance / Å	β or γ / degree			
C(7)–H(7B) $\cdots\pi$ (Cg1)	2.62	12.42 (γ)			1–x, 1–y, 1–z
π (Cg2) $\cdots\pi$ (Cg2)	3.6870(7)	25.7 (β)			1–x, –y, 2–z
Compound 6					
N(1)–H(1A) \cdots N(3)	0.857(19)	2.111(19)	2.9487(16)	165.5(15)	1–x, 1–y, 1–z
N(1)–H(1B) \cdots N(2)	0.835(19)	2.210(19)	2.9810(16)	153.5(17)	1+x, y, z
N(4)–H(4) \cdots O(2)	0.843(19)	2.117(19)	2.9130(15)	157.2(18)	–3/2+x, 1/2–y, –1/2+z
C(5)–H(5) \cdots O(2)	0.95	2.41	3.3152(17)	160	3/2–x, –1/2+y, 3/2–z
C(12)–H(12) \cdots O(1)	0.95	2.44	3.3122(16)	152	1–x, –y, 1–z

^a γ is the Cg–H vector and ring normal; ^b β is the angle between the centroid vector Cg(I) \cdots Cg(J) and the normal to plane I.

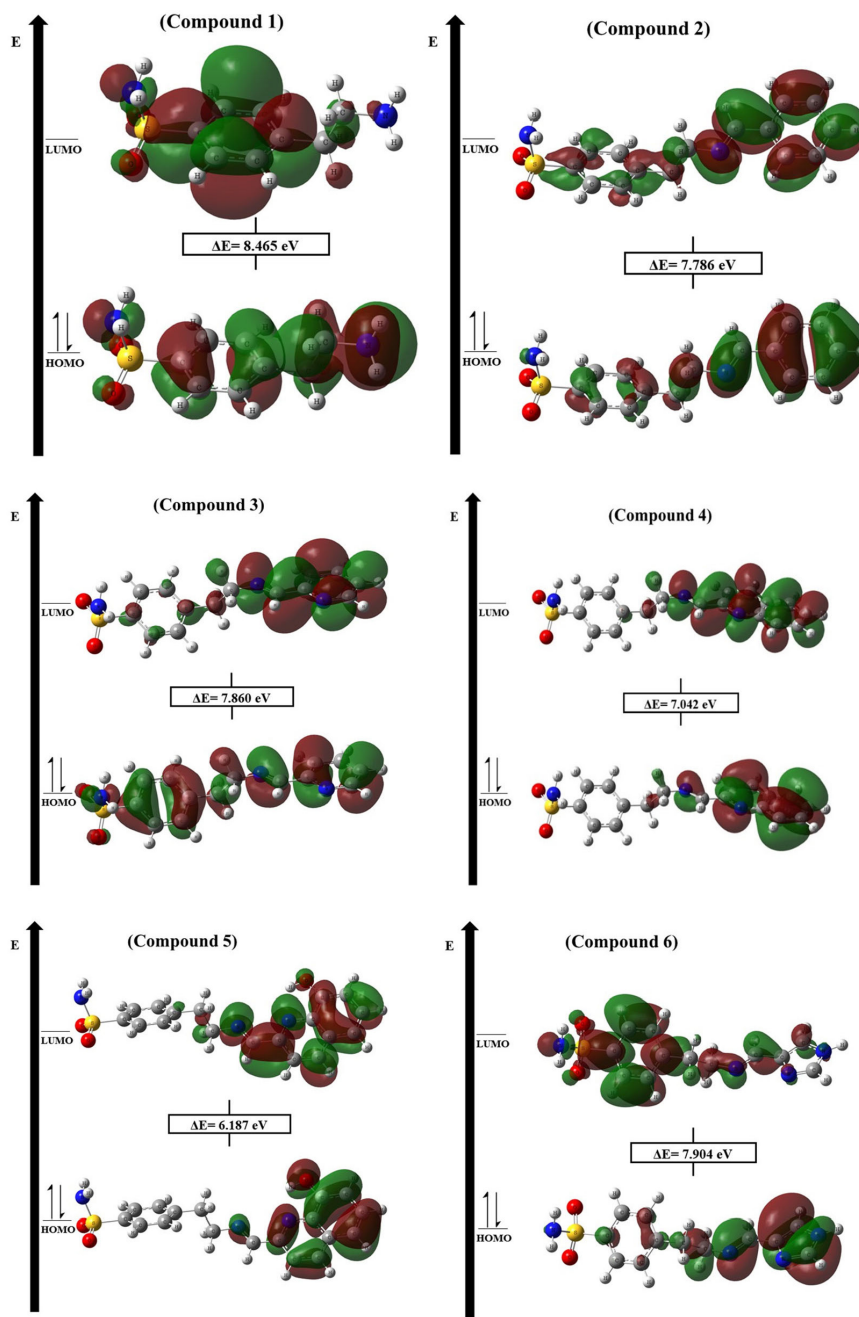


Figure 4. Representation of frontier molecular orbitals (HOMO and LUMO) for compounds 1-6.

compounds **4** and **5**, which indicates, for these compounds, a reduced reactivity in this region. For compound **1**, the free amino group contributes greatly to the HOMO, which is consistent with it being the Lewis base in the formation of the Schiff bases. Additionally, the frontier molecular orbitals indicate contribution of the imine nitrogen atom and of the N-heterocyclic nitrogen atoms (for compounds **3-6**), which indicate the reactive sites.

The obtained HOMO and LUMO energies were used to calculate reactivity indices, such as ionization potential (IP), electron affinity (EA), hardness (η), softness (S), chemical

potential (μ), electronegativity (χ), and electrophilicity index (ω) referring to sulfonamides are shown in Table S3 (SI section). Chemical hardness is an important parameter in investigating the behavior of chemical systems, which indicates the stability of a group of nuclei and electrons in the face of variations in their electronic distribution.^{52,53} As described in Table S3, the chemical hardness determined for the compounds is considerably low, with values below -6.0 eV. The ΔE (energy gap) values can indicate the reactivity/bioreactivity of the molecules, where the lower ΔE value, the more reactive the molecule. The ΔE results

show that compound **5** is the most reactive with a value of $\Delta E = 6.187$ eV, compounds **2**, **3**, **4** and **6** have moderate reactivity and compound **1** is the least reactive for the class studied (compound **1-6**).

The parameters χ and μ measure the power of attracting electrons in addition to highlighting the tendency to lose electrons from a system in equilibrium.⁵⁴⁻⁵⁶ The values obtained for μ and χ for sulfonamides show that the compounds are reactive and present significant electronegativity. The ω showed that sulfonamide **6** (-1.067 eV) is the most electrophilic compound among the others.

The electronic structure of the compounds was further evaluated by recording their UV-Vis spectra in ethanol and using TD-DFT to elucidate the nature of the transitions (see Figure S13, SI section). Comparing the spectra, the trend of the most intense bands is close to the experimental one, but the wavelength range is slightly different due to the error associated with the method. The maximum wavelengths are: $\lambda_{\max, \text{compound } 1} = 187.25$ nm, $\lambda_{\max, \text{compound } 2} = 192.76$ nm, $\lambda_{\max, \text{compound } 3} = 188.99$ nm, $\lambda_{\max, \text{compound } 4} = 236.94$ nm, $\lambda_{\max, \text{compound } 5} = 251.35$ nm, $\lambda_{\max, \text{compound } 6} = 232.84$ nm, which differ from the experimental ones by a maximum of 17 nm.

To explain UV-Vis spectra, 10 excited states were generated and the results of wavelength (nm), oscillator strength, excitation energy (eV), and the highest contributions of molecular orbitals to electronic transitions are presented in Table S4 (SI section). Each transition presented different contributions between the frontier molecular orbitals and the main contributions to each transition are represented by those of the type $\pi \rightarrow \pi^*$.

It is important to highlight that the first transition for compound **5** has a HOMO \rightarrow LUMO contribution of 96%, Table S4 ($\pi \rightarrow \pi^*$), and by analyzing the frontier molecular orbitals it is possible to assess that HOMO and LUMO are located in the same part of the molecule (the 8-hydroxyquinoline ring). The location of the orbitals allows for a lower energy gap value and therefore a higher λ_{\max} . These data indicate the relevance of the 8-hydroxyquinoline motif to the overall reactivity of compound **5**, which could be reflected in its biological properties (see "Biological assays" sub-section).

Biological assays

Finally, compounds **1-6** were screened for their antiviral activity by using a recombinant CHIKV designed for expression of nanoluciferase reporter (CHIKV-*nanoluc*). This construct was used to evaluate the anti-CHIKV activity of the compounds and possesses similar replication rates to the wildtype virus.⁵⁷⁻⁶⁰ First, naive BHK-21 cells

were treated with compounds at 50, 10, and 2 $\mu\text{mol L}^{-1}$ and cell viability was assessed by MTT assay. The results demonstrated that only compound **5** was cytotoxic at 50 $\mu\text{mol L}^{-1}$ (Figures S14, S15, SI section). The highest non-cytotoxic concentration was selected to assess the anti-CHIKV activity of all compounds. Cells were infected with CHIKV-*nanoluc* at a MOI of 0.1 in the presence or absence of each compound and nanoluciferase activity levels, which is proportional to viral replication, were assessed 16 h post-infection.

As observed in Figure 5, all 6 compounds had approximately 50% of viral replication inhibition. Given that compounds **1-4** and **6** had the same activity at 50 $\mu\text{mol L}^{-1}$, it could be related to the initial chemical backbone of the sulfonamide **1**. The only difference was that of compound **5**, which showed the same inhibitory activity, but at 10 $\mu\text{mol L}^{-1}$. This can be related to the effect of the 8-hydroxyquinoline substitution, so that the combination of the sulfonamide and 8-hydroxyquinoline scaffolds could be further investigated for the development of anti-CHIKV compounds. Compound **5** presented activity comparable to other molecules tested against CHIKV, which include the antimalarial drug chloroquine (with half maximal effective concentration (EC_{50}) of 5-11 $\mu\text{mol L}^{-1}$) and the drug used to treat trypanosomiasis suramin (8.8-62.1 $\mu\text{mol L}^{-1}$).⁶¹ 8-Hydroxyquinoline derivatives have been reported as potent inhibitors of dengue virus and West Nile virus proteases,^{62,63} which are validated targets for CHIKV and ZIKV as well.^{64,65}

A similar approach was used to evaluate the anti-ZIKV activity of the compounds, but here employing Vero E6 cells infected with ZIKVPE243 at a MOI of 0.01 in the presence or absence of each compound at the highest non-cytotoxic

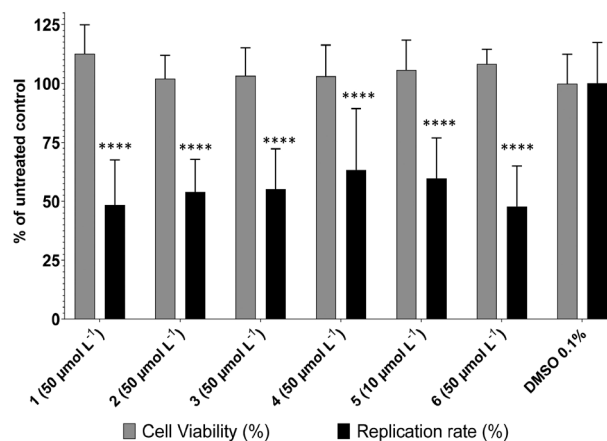


Figure 5. Effect of compounds on BHK-21 viability and CHIKV infection. BHK 21 cells were infected with CHIKV-*nanoluc* and simultaneously treated with compounds at 50 or 10 $\mu\text{mol L}^{-1}$. After 16 h post infection, cells were lysed, and a *Renilla*-luciferase assay was performed to assess CHIKV replication. Mean values of three independent experiments, each measured in triplicate including the standard deviation are shown. DMSO was used as untreated control. **** $P < 0.0001$.

concentration. Again, only compound **5** was cytotoxic at $50 \mu\text{mol L}^{-1}$ to Vero E6 cells. Results of anti-ZIKV activity (Figure 6) were in great contrast to those of anti-CHIKV activity. The compound **6** showed a modest anti-ZIKV activity at $50 \mu\text{mol L}^{-1}$, indicating that the 4-imidazole scaffold might have a role in this antiviral activity. For comparison to other compounds reported in the literature, chloroquine showed an EC_{50} of $10 \mu\text{mol L}^{-1}$ when tested for anti-ZIKV activity in Vero cells, while suramin had an EC_{50} at around $40 \mu\text{mol L}^{-1}$.⁶⁶ Additional studies are envisaged to further evaluate the mechanism by which the compounds present the antiviral activity.

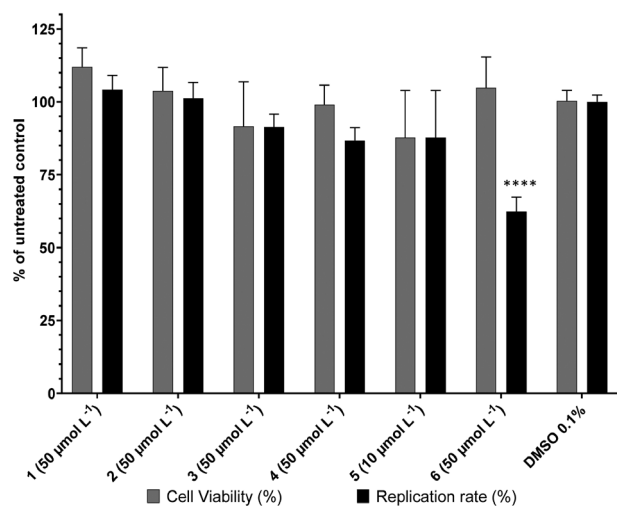


Figure 6. Effect of compounds on Vero E6 cells viability and ZIKV infectivity. Vero E6 cells were infected with ZIKV and simultaneously treated with each compound at the described concentrations. Mean values of two independent experiment each measured in quadruplicate including the standard deviation are shown. *P* values < 0.05 were considered significant.

Conclusions

Synthesis and a comprehensive characterization of five Schiff bases featuring the sulfonamide group were reported in this work. The use of spectroscopic techniques supported by DFT calculations allowed for a detailed analysis of the molecular structures, and the determination of crystal structures provided valuable insights into the supramolecular interactions influenced by the substituent groups of the Schiff bases. The findings underscore the importance of the sulfonamide moiety, with compound **5** demonstrating notable activity against the Chikungunya virus. Contrastingly, only compound **6** displayed (modest) activity against Zika virus. The results not only expand on the structural intricacies of Schiff bases, but also highlight the potential of specific sulfonamide/Schiff bases derivatives as promising chemotypes for further exploration in the development of antiviral agents. Studies to further

explore the potential mechanisms that lead to the biological activity of the compounds are envisaged.

Supplementary Information

Crystallographic data for the structures in this work were deposited in the Cambridge Crystallographic Data Centre as supplementary publication numbers CCDC 2305461-2305465. Copies of the data can be obtained, free of charge, via <https://www.ccdc.cam.ac.uk/structures/>.

Supplementary information (Figures S1-S15, Tables S1-S4) is available free of charge at <http://jbc.sbj.org.br> as PDF file.

Acknowledgments

This work was funded by the Brazilian Council of Technological and Scientific Development (CNPq, grants 407012/2018-4 and 309800/2021-8 to P.P.C.) and the São Paulo Research Foundation (FAPESP, grant No. 2015/20882-3 to D.H.N.; No. 2021/10265-8, Cancer Theranostics Innovation Center CancerThera, CEPID-Centros de Pesquisa, Inovação e Difusão to P.P.C.). DHP acknowledges the Center for Computational Engineering and Sciences (financial support from FAPESP-Fundação de Amparo à Pesquisa, Grant 2013/08293-7, and Grant 2017/11485-6) and the National Center for High Performance Processing (Centro Nacional de Processamento de Alto Desempenho-CENAPAD) in São Paulo for their computational resources. A.C.G.J. is grateful to FAPEMIG (Minas Gerais Research Foundation APQ-01487-22 and APQ-04686-22) and to CAPES (Coordenação de Aperfeiçoamento de Pessoal de Nível Superior-Brasil-Prevention and Combat of Outbreaks, Endemics, Epidemics and Pandemics-Finance Code No. 88881.506794/2020-01 and Finance Code 001. N.M.S. is grateful for CAPES scholarship No. 88887.703845/2022-00. This study was also financed in part by the Coordenação de Aperfeiçoamento de Pessoal de Nível Superior - Brasil (CAPES) - Finance Code 001.

Author Contributions

Douglas H. Nakahata was responsible for conceptualization, data curation, formal analysis, investigation, supervision, validation, visualization, writing-original draft, review and editing; Carlos E. S. P. Corsino for investigation, formal analysis, writing-review and editing; Guilherme C. de Moraes for investigation, formal analysis, writing-review and editing; Gabriele M. Pereira for investigation, formal analysis, writing-review and editing; Álefe B. Cruz for investigation, formal analysis, writing-review and editing; Natasha M. Cassani for investigation, formal analysis, writing-review and

editing; Uriel Enrique A. Ruiz for investigation, formal analysis, writing-review and editing; Igor de Andrade Santos for investigation, formal analysis, writing-review and editing; Douglas Henrique Pereira for data curation, formal analysis, funding acquisition, project administration, resources, supervision, writing-original draft, review and editing; Ana C. G. Jardim for data curation, formal analysis, funding acquisition, project administration, resources, supervision, validation, writing-original draft, review and editing; Pedro P. Corbi for conceptualization, data curation, formal analysis, funding acquisition, project administration, resources, supervision, validation, writing-original draft, review and editing.

References

1. Bartholomeeusen, K.; Daniel, M.; LaBeaud, D. A.; Gasque, P.; Peeling, R. W.; Stephenson, K. E.; Ng, L. F. P.; Ariën, K. K.; *Nat. Rev. Dis. Primer* **2023**, *9*, 17. [Crossref]
2. Pierson, T. C.; Diamond, M. S.; *Nature* **2018**, *560*, 573. [Crossref]
3. Pérez-Pérez, M.-J.; Delang, L.; Ng, L. F. P.; Priego, E.-M.; *Expert Opin. Drug Discovery* **2019**, *14*, 855. [Crossref]
4. Li, K.; Ji, Q.; Jiang, S.; Zhang, N.; *Front. Cell. Infect. Microbiol.* **2022**, *12*, ID 946957. [Crossref]
5. da Silva, S.; Martins, D. O. S.; Jardim, A. C. G.; *Viruses* **2018**, *10*, 255. [Crossref]
6. Martins, D. O. S.; Santos, I. A.; de Oliveira, D. M.; Grosche, V. R.; Jardim, A. C. G.; *Viruses* **2020**, *12*, 272. [Crossref]
7. Wright, P. M.; Seiple, I. B.; Myers, A. G.; *Angew. Chem., Int. Ed.* **2014**, *53*, 8840. [Crossref]
8. Chen, W.-C.; Simanjuntak, Y.; Chu, L.-W.; Ping, Y.-H.; Lee, Y.-L.; Lin, Y.-L.; Li, W.-S.; *J. Med. Chem.* **2020**, *63*, 1313. [Crossref]
9. Ahmed-Belkacem, R.; Hausdorff, M.; Delpal, A.; Sutto-Ortiz, P.; Colmant, A. M. G.; Touret, F.; Ogando, N. S.; Snijder, E. J.; Canard, B.; Coutard, B.; Vasseur, J.-J.; Decroly, E.; Debart, F.; *J. Med. Chem.* **2022**, *65*, 6231. [Crossref]
10. Moskalik, M. Y.; *Molecules* **2023**, *28*, 51. [Crossref]
11. Pacheco, P. A. F.; Gonzaga, D. T.; Cirne-Santos, C. C.; Barros, C. S.; Gomes, M. W. L.; Gomes, R. S. P.; Gonçalves, M. C.; Ferreira, V. F.; Rabelo, V. W.; Abreu, P. A.; Faria, R. X.; de Resende, G. O.; da Rocha, D. R.; Paixão, I. C. N. P.; da Silva, F. C.; *J. Braz. Chem. Soc.* **2022**, *33*, 556. [Crossref]
12. Durgun, M.; Turkmen, H.; Ceruso, M.; Supuran, C. T.; *Bioorg. Med. Chem. Lett.* **2015**, *25*, 2377. [Crossref]
13. Dilworth, J. R.; Pasco, S. I.; Waghorn, P. A.; Vullo, D.; Bayly, S. R.; Christlieb, M.; Sun, X.; Supuran, C. T.; *Dalton Trans.* **2015**, *44*, 4859. [Crossref]
14. McDonald, P. C.; Winum, J.-Y.; Supuran, C. T.; Dedhar, S.; *Oncotarget* **2012**, *3*, 84. [Crossref]
15. Raczuk, E.; Dmochowska, B.; Samaszko-Fiertek, J.; Madaj, J.; *Molecules* **2022**, *27*, 787. [Crossref]
16. Boulechfar, C.; Ferkous, H.; Delimi, A.; Djedouani, A.; Kahlouche, A.; Boublia, A.; Darwish, A. S.; Lemaoui, T.; Verma, R.; Benguerba, Y.; *Inorg. Chem. Commun.* **2023**, *150*, 110451. [Crossref]
17. Hasanzadeh Esfahani, M.; Ghasemi, L.; Behzad, M.; Skorepova, E.; Dusek, M.; *Polycycl. Aromat. Compd.* **2023**, *43*, 8933. [Crossref]
18. Ghasemi, L.; Abedi, A.; Abbasi, A.; Kucerakova, M.; Dusek, M.; Behzad, M.; *Inorg. Chem. Commun.* **2024**, *159*, 111795. [Crossref]
19. Ghasemi, L.; Behzad, M.; Abedi, A.; Khaleghian, A.; *Appl. Organomet. Chem.* **2023**, *37*, e7256. [Crossref]
20. Kaushik, S.; Paliwal, S. K.; Iyer, M. R.; Patil, V. M.; *Med. Chem. Res.* **2023**, *32*, 1063. [Crossref]
21. Maji, M.; Acharya, S.; Bhattacharya, I.; Gupta, A.; Mukherjee, A.; *Inorg. Chem.* **2021**, *60*, 4744. [Crossref]
22. Fulmer, G. R.; Miller, A. J. M.; Sherden, N. H.; Gottlieb, H. E.; Nudelman, A.; Stoltz, B. M.; Bercaw, J. E.; Goldberg, K. I.; *Organometallics* **2010**, *29*, 2176. [Crossref]
23. *APEXII*; Bruker AXS Inc., Madison, Wisconsin, USA, 2012.
24. *SAINT*; Bruker AXS Inc., Madison, Wisconsin, USA, 2012.
25. *SADABS*; Bruker AXS Inc., Madison, Wisconsin, USA, 2001.
26. Sheldrick, G. M.; *Acta Crystallogr., Sect. C: Struct. Chem.* **2015**, *71*, 3. [Crossref]
27. Dolomanov, O. V.; Bourhis, L. J.; Gildea, R. J.; Howard, J. A. K.; Puschmann, H.; *J. Appl. Crystallogr.* **2009**, *42*, 339. [Crossref]
28. Macrae, C. F.; Bruno, I. J.; Chisholm, J. A.; Edgington, P. R.; McCabe, P.; Pidcock, E.; Rodriguez-Monge, L.; Taylor, R.; van de Streek, J.; Wood, P. A.; *J. Appl. Crystallogr.* **2008**, *41*, 466. [Crossref]
29. Frisch, M. J.; Trucks, G. W.; Schlegel, H. B.; Scuseria, G. E.; Robb, M. A.; Cheeseman, J. R.; Scalmani, G.; Barone, V.; Petersson, G. A.; Nakatsuji, H.; Li, X.; Caricato, M.; Marenich, A. V.; Bloino, J.; Janesko, B. G.; Gomperts, R.; Mennucci, B.; Hratchian, H. P.; Ortiz, J. V.; Izmaylov, A. F.; Sonnenberg, J. L.; Williams-Young, D.; Ding, F.; Lipparini, F.; Egidi, F.; Goings, J.; Peng, B.; Petrone, A.; Henderson, T.; Ranasinghe, D.; Zakrzewski, V. G.; Gao, J.; Rega, N.; Zheng, G.; Liang, W.; Hada, M.; Ehara, M.; Toyota, K.; Fukuda, R.; Hasegawa, J.; Ishida, M.; Nakajima, T.; Honda, Y.; Kitao, O.; Nakai, H.; Vreven, T.; Throssell, K.; Montgomery Jr., J. A.; Peralta, J. E.; Ogliaro, F.; Bearpark, M. J.; Heyd, J. J.; Brothers, E. N.; Kudin, K. N.; Staroverov, V. N.; Keith, T. A.; Kobayashi, R.; Normand, J.; Raghavachari, K.; Rendell, A. P.; Burant, J. C.; Iyengar, S. S.; Tomasi, J.; Cossi, M.; Millam, J. M.; Klene, M.; Adamo, C.; Cammi, R.; Ochterski, J. W.; Martin, R. L.; Morokuma, K.; Farkas, O.; Foresman, J. B.; Fox, D. J.; *Gaussian 09*, Revision D.01, Gaussian, Inc., Wallingford CT, 2009.
30. Dennington, R.; Keith, T. A.; Millam, J. M.; *GaussView*, version 6; Semichem Inc., Shawnee Mission, USA, 2016.

31. Stephens, P. J.; Devlin, F. J.; Chabalowski, C. F.; Frisch, M. J.; *J. Phys. Chem.* **1994**, *98*, 11623. [Crossref]
32. Vosko, S. H.; Wilk, L.; Nusair, M.; *Can. J. Phys.* **1980**, *58*, 1200. [Crossref]
33. Becke, A. D.; *J. Chem. Phys.* **1993**, *98*, 5648. [Crossref]
34. Lee, C.; Yang, W.; Parr, R. G.; *Phys. Rev. B* **1988**, *37*, 785. [Crossref]
35. Hehre, W. J.; Stewart, R. F.; Pople, J. A.; *J. Chem. Phys.* **1969**, *51*, 2657. [Crossref]
36. Ditchfield, R.; Hehre, W. J.; Pople, J. A.; *J. Chem. Phys.* **1971**, *54*, 724. [Crossref]
37. Krishnan, R.; Binkley, J. S.; Seeger, R.; Pople, J. A.; *J. Chem. Phys.* **1980**, *72*, 650. [Crossref]
38. Parr, R. G.; Donnelly, R. A.; Levy, M.; Palke, W. E.; *J. Chem. Phys.* **2008**, *68*, 3801. [Crossref]
39. Duarte, H. A.; *Quim. Nova* **2001**, *24*, 501. [Crossref]
40. Yanai, T.; Tew, D. P.; Handy, N. C.; *Chem. Phys. Lett.* **2004**, *393*, 51. [Crossref]
41. Marenich, A. V.; Cramer, C. J.; Truhlar, D. G.; *J. Phys. Chem. B* **2009**, *113*, 6378. [Crossref]
42. Barnes, L.; Schindler, B.; Allouche, A.-R.; Simon, D.; Chambert, S.; Oomens, J.; Compagnon, I.; *Phys. Chem. Chem. Phys.* **2015**, *17*, 25705. [Crossref]
43. Pohjala, L.; Utt, A.; Varjak, M.; Lulla, A.; Merits, A.; Ahola, T.; Tammela, P.; *PLoS One* **2011**, *6*, e28923. [Crossref]
44. Matkovic, R.; Bernard, E.; Fontanel, S.; Eldin, P.; Chazal, N.; Hassan Hersi, D.; Merits, A.; Péloponèse, J.-M.; Briant, L.; *J. Virol.* **2019**, *93*. [Crossref]
45. Donald, C. L.; Brennan, B.; Cumberworth, S. L.; Rezelj, V. V.; Clark, J. J.; Cordeiro, M. T.; Freitas de Oliveira França, R.; Pena, L. J.; Wilkie, G. S.; Da Silva Filipe, A.; Davis, C.; Hughes, J.; Varjak, M.; Selinger, M.; Zuvanov, L.; Owsianka, A. M.; Patel, A. H.; McLauchlan, J.; Lindenbach, B. D.; Fall, G.; Sall, A. A.; Biek, R.; Rehwinkel, J.; Schnettler, E.; Kohl, A.; *PLoS Neglected Trop. Dis.* **2016**, *10*, e0005048. [Crossref]
46. Cassani, N. M.; Santos, I. A.; Grosche, V. R.; Ferreira, G. M.; Guevara-Vega, M.; Rosa, R. B.; Pena, L. J.; Nicolau-Junior, N.; Cintra, A. C. O.; Mineo, T. P.; Sabino-Silva, R.; Sampaio, S. V.; Jardim, A. C. G.; *Int. J. Biol. Macromol.* **2023**, *227*, 630. [Crossref]
47. *International Tables for Crystallography*, vol. C, 3rd ed.; Prince, E., ed.; Kluwer Academic: Dordrecht, 2004.
48. Coombs, R. R.; Ringer, M. K.; Blacquiére, J. M.; Smith, J. C.; Neilsen, J. Scott.; Uh, Y.-S.; Gilbert, J. Bryson.; Leger, L. J.; Zhang, H.; Irving, A. M.; Wheaton, S. L.; Vogels, C. M.; Westcott, S. A.; Decken, A.; Baerlocher, F. J.; *Transit. Met. Chem.* **2005**, *30*, 411. [Crossref]
49. Chohan, Z. H.; Shad, H. A.; Tahir, M. N.; Thebo, K. H.; *Acta Crystallogr., Sect. E: Struct. Rep. Online* **2009**, *65*, o2450. [Crossref]
50. Mahmood, K.; Yaqub, M.; Tahir, M. N.; Shafiq, Z.; Qureshi, A. M.; *Acta Crystallogr., Sect. E: Struct. Rep. Online* **2010**, *66*, o2436. [Crossref]
51. Jumabaev, A.; Holikulov, U.; Hushvaktov, H.; Issaoui, N.; Absanov, A.; *J. Mol. Liq.* **2023**, *377*, 121552. [Crossref]
52. Devi, D.; Arasu, M. M. A.; Giriya, A. M.; *J. Indian Chem. Soc.* **2022**, *99*, 100400. [Crossref]
53. Kaviani, S.; Izadyar, M.; Housaindokht, M. R.; *Polyhedron* **2016**, *117*, 623. [Crossref]
54. Domingo, L. R.; Pérez, P.; *Org. Biomol. Chem.* **2011**, *9*, 7168. [Crossref]
55. Costa, R. A.; da Silva, J. N.; Oliveira, V. G.; Anselmo, L. M.; Araújo, M. M.; Oliveira, K. M. T.; Nunomura, R. C. S.; *J. Mol. Liq.* **2021**, *330*, 115625. [Crossref]
56. Bhattacharya, A.; Naskar, J. P.; Saha, P.; Ganguly, R.; Saha, B.; Choudhury, S. T.; Chowdhury, S.; *Inorg. Chim. Acta* **2016**, *447*, 168. [Crossref]
57. Santos, I. A.; Pereira, A. K. S.; Guevara-Vega, M.; de Paiva, R. E. F.; Sabino-Silva, R.; Bergamini, F. R. G.; Corbi, P. P.; Jardim, A. C. G.; *Acta Trop.* **2022**, *227*, 106300. [Crossref]
58. de Oliveira, D. M.; Santos, I. A.; Martins, D. O. S.; Gonçalves, Y. G.; Cardoso-Sousa, L.; Sabino-Silva, R.; Von Poelhsitz, G.; Franca, E. F.; Nicolau-Junior, N.; Pacca, C. C.; Merits, A.; Harris, M.; Jardim, A. C. G.; *Front. Microbiol.* **2020**, *11*, 608924. [Crossref]
59. Santos, I. A.; Shimizu, J. F.; de Oliveira, D. M.; Martins, D. O. S.; Cardoso-Sousa, L.; Cintra, A. C. O.; Aquino, V. H.; Sampaio, S. V.; Nicolau-Junior, N.; Sabino-Silva, R.; Merits, A.; Harris, M.; Jardim, A. C. G.; *Sci. Rep.* **2021**, *11*, 8717. [Crossref]
60. Ruiz, U. E. A.; Santos, I. A.; Grosche, V. R.; Fernandes, R. S.; de Godoy, A. S.; Torres, J. D. A.; Freire, M. C. L. C.; Mesquita, N. C. M. R.; Guevara-Vega, M.; Nicolau-Junior, N.; Sabino-Silva, R.; Mineo, T. W. P.; Oliva, G.; Jardim, A. C. G.; *Virus Res.* **2023**, *324*, 199029. [Crossref]
61. Hucke, F. I. L.; Bugert, J. J.; *Front. Public Health* **2020**, *8*, 618624. [Crossref]
62. Lai, H.; Sridhar Prasad, G.; Padmanabhan, R.; *Antiviral Res.* **2013**, *97*, 74. [Crossref]
63. Ezgimen, M.; Lai, H.; Mueller, N. H.; Lee, K.; Cuny, G.; Ostrov, D. A.; Padmanabhan, R.; *Antiviral Res.* **2012**, *94*, 18. [Crossref]
64. Ivanova, L.; Rausalu, K.; Ošeka, M.; Kananovich, D. G.; Žusinaite, E.; Tammiku-Taul, J.; Lopp, M.; Merits, A.; Karelson, M.; *ACS Omega* **2021**, *6*, 10884. [Crossref]
65. Quek, J. P.; Liu, S.; Zhang, Z.; Li, Y.; Ng, E. Y.; Loh, Y. R.; Hung, A. W.; Luo, D.; Kang, C.; *Antiviral Res.* **2020**, *175*, 104707. [Crossref]
66. Baz, M.; Boivin, G.; *Pharmaceuticals* **2019**, *12*, 101. [Crossref]

Submitted: January 9, 2024

Published online: April 8, 2024